

MODELING AND ANALYSIS OF DIGITAL SURFACE MODELS USING HIGH-RESOLUTION UAV IMAGES

MODELIRANJE IN ANALIZA DIGITALNIH POVRŠINSKIH MODELOV Z UPORABO VISOKO LOČLJIVIH UAV SLIK

Andrej Pal

University of Ljubljana,
Faculty of Natural Sciences and Engineering,
Department of Geotechnology, Mining and
Environment
Aškerčeva 12, 1000 Ljubljana, Slovenia
E-mail: andrej.pal@ogr.ntf.uni-lj.si

Mirko Borisov

University of Novi Sad,
Faculty of Technical Sciences
Trg Dositeja Obradovića 6, 21000 Novi Sad,
Republic of Serbia
E-mail: mborisov@uns.ac.rs

Milivoj Vulić

University of Ljubljana,
Faculty of Natural Sciences and Engineering,
Department of Geotechnology, Mining and
Environment
Aškerčeva cesta 12, 1000 Ljubljana, Slovenia
E-mail: milivoj.vulic@guest.arnes.si

DOI <https://doi.org/10.18690/actageotechslov.17.1.46-55.2020>

Keywords

digital photogrammetry, UAV, GNSS measurements, point cloud, DSM

Ključne besede

digitalna fotogrametrija, meritve UAV, meritve GNSS, oblak točk, DSM

Abstract

Unmanned aerial vehicles (UAVs) are increasingly used for geodata collection and topographic mapping. The use of UAVs in photogrammetric surveying provides an effective way to obtain orthophotographs and digital surface models (DSMs). Detailed investigations can be carried out in inaccessible parts of the observed area, such as steep slopes, muddy and silty terrain, locations with high risk, etc. There are various software packages for the processing of UAV photogrammetric-based data. In this study, 618 high-resolution images of an open-pit excavation were obtained with an Anafi Parrot-type UAV from a height of approximately 30 m. The ground control points were established with customized markers and fast static GNSS measurements. The high-resolution images were processed using two software tools: Agisoft Metashape Professional and Pix4Dmapper Pro. From the produced high-density 3D point clouds, DSMs, orthomosaics and digital elevation models (DEMs) were developed. The quality of the UAV-produced digital models was assessed by a comparison with terrestrial measurements, where the focus was on water areas that cause noise on the model surface.

Izvleček

Brezpilotna letalska vozila (UAV) se vedno pogosteje uporabljajo za zbiranje geodetskih podatkov in topografsko kartografijo. Uporaba UAV-jev pri fotogrametričnem raziskovanju zagotavlja učinkovit način za pridobivanje ortofotografij in digitalnih površinskih modelov (DSM). Podrobne preiskave se lahko izvajajo na nedostopnih delih opazovanega območja, kot so strma pobočja, blatni in močvirni teren, lokacije z visokim tveganjem itd. Obstajajo različni programski paketi za obdelavo podatkov na podlagi fotogrametričnih podatkov UAV. V tej raziskavi je bilo z UAV tipom Anafi Parrot z višine približno 30 m pridobljenih 618 posnetkov visoke ločljivosti izkopa odprte gradbene jame. Vzpostavljene so bile talne kontrolne točke s prilagojenimi označevalci in hitrimi statičnimi meritvami GNSS. Slike z visoko ločljivostjo so bile obdelane z uporabo dveh programskih orodij: Agisoft Metashape Professional in Pix4Dmapper Pro. Iz proizvedenih 3D točkovnih oblakov visoke gostote smo razvili modele DSM, otomozaike in digitalne višinske modele (DEM). Kakovost digitalnih modelov, ki jih proizvajajo UAV, je bila ocenjena s primerjavo z zemeljskimi meritvami, kjer je bil poudarek na vodnih območjih, ki povzročajo hrup na površini modela.

1 INTRODUCTION

Aerial imagery has long been used in geodesy and cartography to obtain an overhead view of terrain, infrastructure, and to situate sites within the visual and physical landscape. This was accomplished by placing cameras on the hull of aircraft or other utility vehicles with extendable platforms [1, 2]. In the past decade, technological advances have allowed air-bound surveying techniques to be re-established in practical terms and are nowadays extensively applied in the process of digital 3D terrain modeling [3-16]. In a variety of engineering disciplines, affordable and flexible unmanned aerial vehicles (UAVs) are being used to obtain high-resolution remote-sensing data of larger (observational) areas on the Earth's surface. An UAV-based photogrammetry technique allows multi-temporal, multi-spectral imagery in a fast, cost-effective and simple way [3, 4]. Therefore, many researchers explored these recent developments in numerous studies, such as: monitoring terrain deformations [5-7], surveying construction projects [8, 9], characterization of geological features within mining areas [10], abandoned-mine risk assessment [11, 12], highly accurate 3D modeling of mining excavation sites [13-15] or of cultural heritage [16], precise farming [3], etc. These applications require high-resolution, geospatial information and very high accuracy. The accuracy of the produced orthophoto and digital terrain model (DTM) mostly depends on the obtained raw images and the photogrammetric processing methods, such as Structure from Motion (SfM) [17-19].

SfM uses mathematics and digital pattern recognition to calculate the distance/direction of the motion between multiple overlapping images and to triangulate the surface points for geometry reconstruction. It is different to traditional photogrammetric methods because SfM generates positions in an arbitrary coordinate system and requires a georeferencing strategy [17]. Georeferencing can be done directly by using UAV onboard sensors to calculate the camera coordinates at the exact moment of the measurement (photograph acquirement), or indirectly by establishing recognizable ground control points (GCPs), the coordinates of which are known [18]. When using GCPs, an accuracy issue arises in relation to the distribution and the number of points. Even though there are no general GCP positioning rules, Harwin and Lucieer [19] showed that the biggest impact of GCP distribution is in areas with significant relief features. According to their findings, the GCPs should be evenly spread throughout the observation area so that the individual points are spaced at a distance of 1/5 to 1/10 of the UAV flight height,

while on steeper parts of the terrain the distance is reduced. Coordinates of GCPs can be obtained by using Global Navigation Satellite System (GNSS) surveying techniques, allowing an average GCP accuracy at the cm level [20]. In critical areas of the terrain, where the GNSS measurements cannot be carried out, GCPs can be determined using a terrestrial laser scanner (TLS). Additionally, the improved accuracy of the obtained coordinates (at the mm level) from the combination of photogrammetry and TLS contributes to the quality of the generated orthophotos and 3D models, as reported by Tong et al. [15]. The application of SfM, georeferencing, 3D point cloud and digital surface model (DSM) development can all be done with various software packages. Aicardi et al. [16] focused on free and commercial photogrammetric software solutions and based on a verification with LiDAR data, they confirmed that Agisoft Photoscan Professional and Pix4D are best suited to conventional applications, as well as producing good results.

The main purpose of this study was the modeling and analysis of digital surface models (DSMs). Using high-resolution images acquired from photogrammetric UAV surveying, and two software packages, digital models of the observation area were produced. The visual confirmation of the DSMs was done with the obtained images, while for the quantitative assessment, terrestrial measurements were carried out. By comparing UAV and terrestrial-based digital models, the verification was performed on critical areas (water bodies) and along transversal profiles.

2 METHOD AND TECHNOLOGY OF THE STUDY

2.1 Case-study area

The observational, case-study area is located in the eastern part of the Autonomous Province of Vojvodina, in the north Republic of Serbia. Namely, it is the Central Banat District, the cadastral municipality of Novi Bečej, on the eastern border of the construction zone near the city area called "Garajevac" (Fig. 1).

There is not much vegetation in the observed area, so the surface of the soil is clayey with smaller areas of low vegetation or grass, which was very convenient from the viewpoint of the UAV photogrammetry application. The observational area was divided into three smaller areas of interest, as shown in Fig. 2, which were numbered and named on the basis of their characteristics: 1. main excavation pit; 2. the tailings pond and 3. northeastern excavation pit.

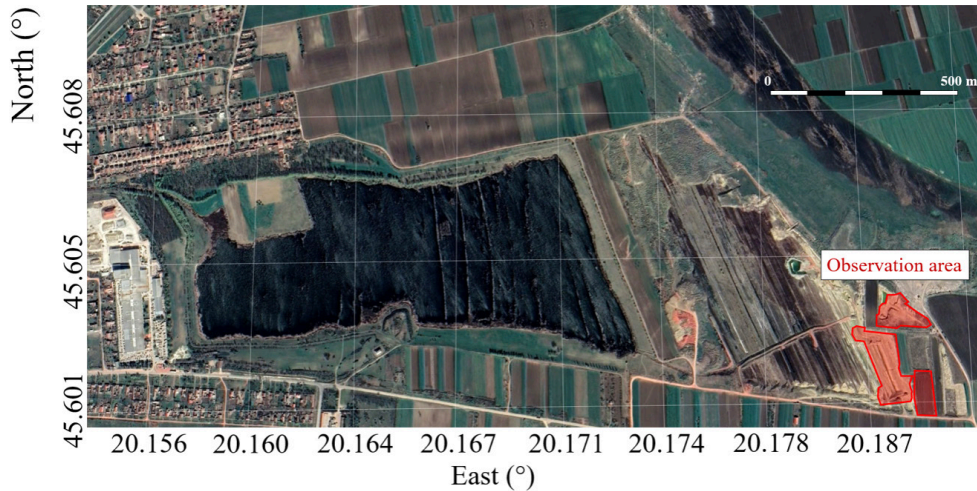


Figure 1. Location of the observational area on the in the construction zone near the city Novi Bečej, Autonomous Province of Vojvodina in the north Republic of Serbia.



Figure 2. Three smaller areas of interest within the observational area.

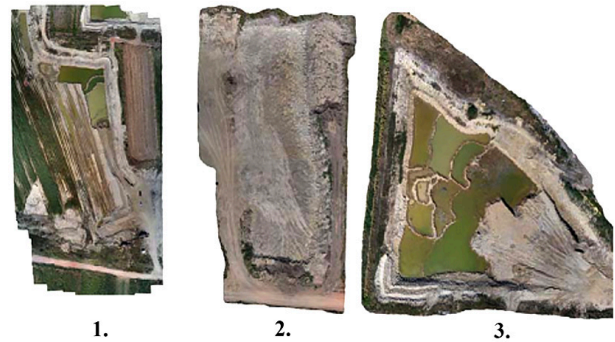


Figure 3. Terrain characteristics of each of the smaller observational areas.

The division of the area into three locations was made primarily because of the limitations dictated by the instrument's performance (UAV) and the hardware requirements for processing and analyzing data. Furthermore, the area division was executed due to the terrain configuration and the characteristics within each individual location (Fig. 3).

1. Main excavation pit - land is covered with clay and low occasional vegetation on the perimeter. Several larger water surfaces cover the area. From the shape of the excavation a saw-tooth-like profile of the terrain remains in some locations.
2. The tailings – land is covered with clay, soil and fine dust. Due to the excavation procedures, the surface is

approximately flat with abrupt changes as it approaches the perimeter dirt roads.

3. Northeast excavation pit – land is covered with clay and the vegetation is low and sparse alongside the perimeter. On the west side there is a field of sunflowers and on the north side there is a waste landfill. The excavation formed a land ramp that goes down to the lowest parts of the excavation pit, while the edges of the land are very sharp. Several larger water surfaces are also spread out in this area.

Also, for this area, periodic surveying of the terrain was conducted in order to monitor changes on the excavation pit's surface, mainly for the purpose of determining the volume of excavated clay and the estimation of raw-material reserves for future excavations. The observational area was suitable for low UAV flights and 3D models due to its flat topography. The highest point of the observational area was 80 m (above sea level), while the lowest part was 69 m.

2.2 UAV and camera

The four-rotor quadcopter UAV, type Anafi Parrot and equipped with a Camera Locations, which was used for this project, is shown in Fig. 4. A three-axis gimbal made it possible to take pictures from different angles and directions. Manual or autonomous navigation was managed with a Parrot Skycontroller 3 flight controller.



Figure 4. Unmanned aerial vehicle (UAV) Anafi Parrot.

The 24 megapixel camera equipped with a rolling shutter was adjusted to take one image every 2 seconds, resulting in a database of more than 618 images with a resolution of 4608×3456.

Both oblique and vertical photographs were taken in the observational area. The image calibration was 100 % (618/618 images calibrated). The flight was carried out at a height of 30 m above the average height of the terrain.

2.3 Ground control points and check points

In order to determine the spatial location of the 9 GCPs, a fast static GNSS survey was conducted. Each GCP was observed for 20 minutes in fast static GNSS mode, using three Trimble R10 GNSS instruments [21]. This allowed us to obtain valid horizontal coordinates with an accuracy of 3 mm + 0.5 ppm. The RMS precision in a horizontal and 5 mm + 0.5 ppm RMS precision in a vertical position in fast static surveying. For the block adjustment, georeferenced orthophotos and the DSM development, a total of 23 GCPs were used. Absolute accuracy was tested with 26 checkpoints (CPs) that were established in the observational area (Fig. 5). Red-and-white painted metal plates were used as the GCPs and CPs (Fig. 5 and 6).

Leica Geo Office (LGO 2.0) software was used to process the GNSS signals and obtain precise coordinates for the observed points.

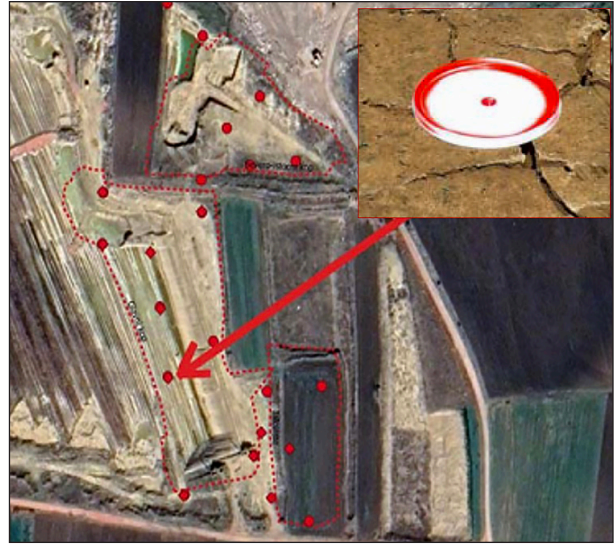


Figure 5. Layout of ground control points (GCPs) within the observational area. Type of marker (red-and-white plate) is presented in the top-right corner.



Figure 6. Positioning marker for GCP or CP.

The coordinates of the check points were calculated by taking the average of the two observations of 5 epochs with a recording interval of 1 second. The coordinates of the 26 CPs are presented in Table 1 (next page).

Problems with the image block absolute positioning within the chosen coordinate frame as well as problems with the deformation effects of the camera's systematic errors, can be solved with an appropriate distribution of the GCP [22]. As a result of the fast static adjustment, the horizontal was 0.01 m and the vertical accuracy was 0.03 m.

Table 1. The coordinates (x,y,z) of 26 check points (CPs).

ID	x (m)	y (m)	z (m)
o1	7436695.67	5051084.59	77.23
k1	7436695.12	5051084.29	77.22
k2	7436643.42	5051058.71	77.15
o2	7436644.09	5051059.11	77.13
o3	7436632.47	5051137.34	70.11
k3	7436632.75	5051136.59	70.11
o4	7436627.22	5051183.44	70.09
k4	7436627.57	5051182.29	70.09
o5	7436585.07	5051225.70	70.06
k5	7436585.67	5051225.63	70.06
k6	7436620.58	5051219.71	70.61
o7	7436666.29	5051160.47	76.96
o8	7436658.72	5051245.78	76.87
o10	7436658.53	5051267.17	79.07
o11	7436694.74	5051276.42	76.09
o12	7436728.15	5051278.95	76.03
o13	7436677.70	5051301.45	71.68
o14	7436702.28	5051322.14	72.73
o15	7436660.59	5051362.67	75.18
o16	7436634.71	5051384.64	75.27
o17	7436705.42	5051127.03	77.19
o18	7436745.88	5051129.90	77.99
o19	7436735.82	5051040.62	78.22
k7	7436707.93	5051056.45	77.54
k10	7436721.70	5051088.89	76.90
k11	7436701.06	5051099.65	77.21

2.4 Flight control

The flight control equipment included an UAV controller in the form of a mobile phone on which a drone-movement-management application and a flight-mission-planning application were installed. Specifically, in our case the Pix4D Capture application was used. The flight control station was established at one of the highest points in the observational area. The flight lasted for approximately 10 minutes. During the flight the mobile phone enabled simultaneous verification of the obtained images. To provide a desired location resolution of 0.02 m or less, the flight height was planned to be approximately 30 m and the overlap rates were 80 % overlapping and 70 % sidelap covering. According to the calculations performed in Pix4D and Agisoft the GSD (Ground Sample Distance) of the data is approximately 0.80 cm and 0.82 cm respectively.

3 PROCESSING OF DATA

Pix4Dmapper Pro [23] and Agisoft Metashape Professional [24] were used in the photogrammetric process chains to produce orthophoto and DSM in ITRF (International Terrestrial Reference Frame) datum.

The collected data are images of the observed clayey terrain within an open pit. Initially, all the images were uploaded, then a visual inspection of those that were located on the perimeter was performed, and by recognizing the details of each image, those that covered any terrain beyond our area of interest were removed. The relevant images were imported into both software packages. With Pix4Dmapper the Initial Processing tool was applied, while with Agisoft Metashape we applied the Align Photos tool. In both cases it was possible to set the image size in which the similarity points were searched. After starting the matching process, a cloud of reference tie-points is formed. The latter is not the final targeted point cloud for surface modeling, but it serves to identify two or more images and improve the fit between them. Following the matching process, the next step is to optimize the shots by referencing the coordinates of the GCPs. A list is loaded into the program coordinates, which were previously derived from the GNSS controllers in CSV format.

The image-matching process generated a cloud made up of matching points, which is a preliminary point cloud with a less-frequent density, and from the camera positions and the calculated-depths information, the generation of a high-density point cloud. The generated point clouds with a given level of detail to ‘medium’, in terms of application and quality, are acceptable for further analyses. A dense point cloud was generated for every observation area, as shown in Fig. 7.

The created terrain models in the form of point clouds, such as the results show, result in huge amounts of data [25]. More specifically, the data of such a structure are reflected in a huge number of points, each with its own spatial position and possibly an attached RGB color code, determined by the snapshot from which the data originates. It is this massive quantity of data that is gaining importance in the modern approach to 3D modeling of real objects [26]. From a geodesy point of view, this kind of data structure should be considered as raw data, which, while very faithfully representing reality, also provides a large number of manipulation options for targeted use.

The software packages enable the transformation of models in the point-cloud structure into a series of others, where each derived model can then be exported to a multitude of data formats. In the domain of digital

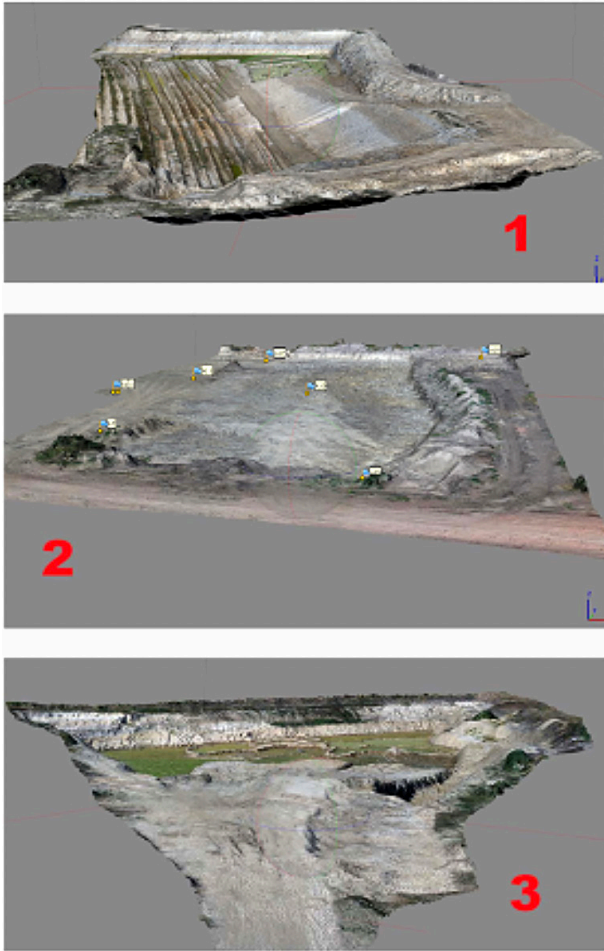


Figure 7. High density 3D point cloud for each observational area.

terrain models, one standard way of interpretation is the DSM structure. The acquisition of UAV data by a diameter system made it possible to obtain a point cloud that displays, in addition to the surface area, the objects on it. The spatial resolution of the digital model is directly related to the level of detail that created the dense cloud point, so the transformation comes down to a choice of projection planes, boundaries, and interpolation modes. For all three projection areas of interest, the chosen map

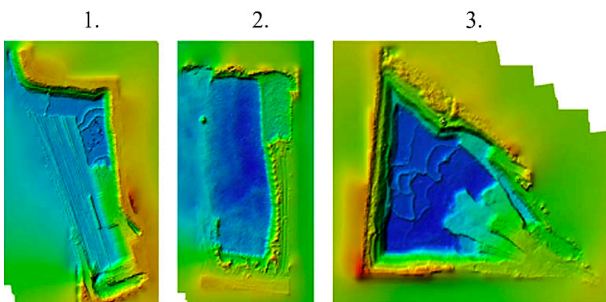


Figure 8. Digital elevation model (DEM) for each observational area.

projections were used, i.e., UTM Zone 34N, geodetic system ETRS89 (Fig. 8).

Twenty-six CPs were used for georeferencing. The coordinates of the dense point cloud were obtained from the photogrammetric process and were referred to as UTM Zone 34N (ETRS89) and the elevation set at Mean Sea Level (MSL) by using the EGM08 geoid model. The coordinates of the 26 CPs, measured by RTK control (Real Time Kinematics GNSS) observations, were compared with the coordinate values obtained from both software programs (Agisoft and Pix4D). A number of overlapping images were computed for each orthomosaic pixel (Fig. 9).



Figure 9. Orthomosaic for each observational area.

Running the procedure opens up a dialog to adjust the projection, which is same as with DEM, reconstructed model source (DEM, MESH) and defining pixel sizes whose standard value is identical to the pixel size for the original photographs. According to the desired usage, the resolution can be optimized with the hardware. The export formats for a model structured this way are: *.TIFF, *.JPEG, *.PNG, *.KMZ, World Wind Tiles (*.Zip) and many more.

4 RESULTS AND DISCUSSION

The orthophoto and DSM were produced from high-resolution UAV images using Agisoft Metashape Professional and Pix4Dmapper Pro software. Aerial images were taken at heights between 30 and 35 m with 80 % overlapping and 70 % sidelap covering, and were scaled by precisely coordinated locations using static GNSS observations.

Visual inspection is one of the basic controls of the produced DSM. Given the extensiveness and size of the data that was obtained with the UAV photogrammetric techniques, the produced 3D models were very realistic (Fig. 10). Any texture irregularities or model deviations could be easily identified.

Therefore, we can assume that the formed digital model is of satisfactory quality (Table 2).

Table 2. Control points on the water surface.

ID	Elevation GNSS (m)	Elevation UAV DSM (m)	ΔH (m)
water_2	69.92	69.76	0.16
water_3	69.92	69.85	0.07
water_4	69.92	69.69	0.23
water_5	69.92	69.69	0.23
water_6	69.92	69.71	0.21
water_7	69.92	69.69	0.23
water_8	69.92	69.67	0.25

For the purpose of a comparative analysis of the UAV digital model with the model and maps, based on terrestrial measurements, the surface points were vectorized and shown in Fig. 14.



Figure 14. Vectorization of the 3D terrain model.

These points are of most interest because they are the spatial positions for terrestrial determination. So, the idea was to vectorize the points on the UAV terrain model in the immediate vicinity of the terrestrial points. By selecting the vectorization option, the points on the model are selected, where it is again the best view for vectorization via orthomosaics for realism. In addition to vectorization of the points, it is possible to do the same with lines and polygons, but this geometric format was selected according to the comparative analysis described.

The model of location 3 (the northeast excavation pit) contains a total of 70 vectorized points. Their height differences between the terrestrial and the UAV DEM measurements are given in Table 3.

Table 3. Heights from GNSS measurements (I), heights from DEM UAV (II), surface type (III) and height differences (IV).

ID	I	II	III	IV
1	69.66	69.18	Water	48
2	69.68	69.14	Water	54
3	69.65	69.47	Water	18
4	70.05	69.83	Water	21
5	70.20	70.17	Clay	3
6	70.04	70.13	Water	-9
7	70.08	69.91	Water	17
8	70.13	69.66	Water	47
9	70.11	69.78	Water	33
10	70.11	69.66	Water	45
11	69.61	69.26	Water	35
12	69.70	69.48	Water	22
13	69.59	69.06	Water	53
14	69.59	69.07	Water	52
15	71.12	71.13	Clay	-1
16	71.39	71.33	Clay	6
17	71.61	71.41	Clay	20
18	72.19	72.02	Clay	17
19	74.88	74.97	Clay	-10
20	76.04	76.07	Clay	-4
21	74.82	74.86	Clay	-5
22	76.02	76.03	Clay	-1
23	76.15	76.18	Clay	-3
24	76.11	76.10	Clay	1
25	72.60	72.55	Clay	6
26	74.18	74.17	Clay	1
27	72.84	72.74	Clay	11
28	73.66	73.68	Clay	-3
29	75.36	75.37	Clay	-1
30	72.22	72.13	Clay	9
31	72.45	72.28	Clay	17
32	71.87	71.77	Clay	10
33	71.89	71.81	Clay	8
34	72.53	72.56	Clay	-3
35	72.22	72.09	Clay	13
36	75.83	75.83	Clay	0
37	75.94	75.95	Clay	-1
38	75.94	75.94	Clay	0
39	75.96	75.79	Clay	17
40	75.25	74.94	*LV	30
41	75.26	75.09	Clay	18
42	75.01	74.93	Clay	8
43	74.86	74.62	Clay	24
44	74.85	74.65	Clay	20
45	74.60	74.58	Clay	2
46	75.04	74.97	Clay	7
47	71.79	71.69	Clay	10
48	71.83	71.75	Clay	8
49	73.48	73.48	Clay	0
50	75.35	74.88	*LV	47
51	74.86	74.97	Clay	-11
52	74.98	74.92	Clay	6
53	75.37	75.38	Clay	-1
54	75.30	75.27	Clay	3
55	74.83	74.93	Clay	-10
56	71.80	71.57	Clay	23
57	70.06	69.81	Clay	25
58	70.43	70.26	Clay	17
59	72.40	72.58	Clay	-19
60	72.43	72.45	Clay	-2
61	72.73	72.66	Clay	7
62	72.43	72.40	Clay	3
63	72.49	72.34	Clay	15
64	75.22	75.19	Clay	2
65	75.62	75.56	Clay	6
66	77.44	77.22	*LV	22
67	72.99	72.95	Clay	3
68	75.91	75.93	Clay	-2
69	75.34	75.36	Clay	-2
70	76.23	76.24	Clay	-1

I - elevation GNSS (m); II - elevation DEM (m); III - surface type; IV - height difference (cm); *LV - low vegetation.

In addition, quantitative analyses were considered for the terrestrial and UAV DEM results by profiles. Namely, the terrain profiles in the same area were extracted from the different DEMs and then compared. A comparison of the terrestrial and UAV-based DEM is shown in Fig. 15.

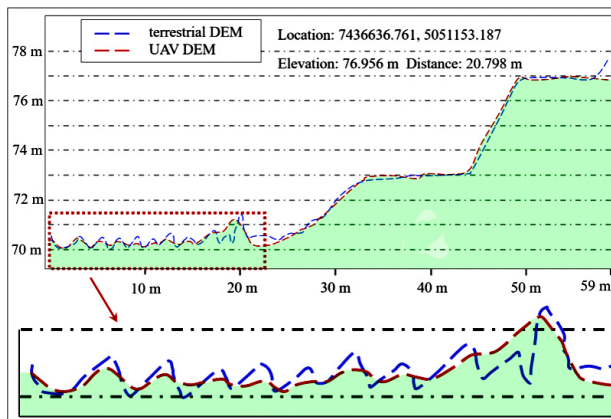


Figure 15. Comparison of terrestrial and UAV-based DEM.

The two DEMs are considered as a good approximation. Some differences occur on the water area and sharp crossings of the terrain. Special attention was given to areas covered with water bodies, because there is the greatest noise on the model. The noise is smaller immediately adjacent to the land boundary and it grows, moving towards the center of the water surface.

5 CONCLUSIONS

This study was carried out to obtain high-quality DSMs with an accuracy and precision at the centimeter level. Agisoft Metashape Professional and Pix4Dmapper Pro were used to process the UAV-based photogrammetric high-resolution images, where both software packages produced satisfactory GSD values. At the 26 GCP locations, which were determined by the GNSS measures, the GSD value was calculated as 0.5 cm/pixel with the Agisoft software, while the Pix4D software calculated it as 0.42 cm/pixel. In the resulting 3D point clouds, large noise was observed at the surfaces that were covered with water bodies and denser vegetation. This negative phenomenon slightly improves when generating the digital model, but in some places unrealistic model peaks remain. Nevertheless, when comparing the terrestrial and UAV-based DEM, a good match is shown in areas where no water bodies are present.

UAV-based photogrammetry has clear advantages over piloted aircraft, satellites and traditional surveying

methods, particularly because of the low cost, operational flexibility, better spatial and temporal resolution, and because it requires less time than other techniques for data acquisition. Such approaches can be efficiently applied in situations where classic photogrammetric surveying is not possible.

Acknowledgments

This study was conducted with the support of the research program P2-0268 and the Slovenian Research Agency. The authors are grateful to the anonymous reviewers and members of the editorial team for their comments.

REFERENCES

- [1] Burnside, C.D. 1985. The future prospects of data acquisition by photographic and other airborne systems for large scale mapping. *The Photogrammetric Record* 11(65), 495-506. DOI: 10.1111/j.1477-9730.1985.tb00519.x
- [2] Hsieh, Y.C., Perlant, F., McKeown, D.M. 2015. Recovering 3D information from complex aerial imagery. in *Proceedings - International Conference on Pattern Recognition*.
- [3] Candiago, S., et al. 2015. Evaluating multispectral images and vegetation indices for precision farming applications from UAV images. *Remote Sensing* 7(4), 4026-4047. DOI: 10.3390/rs70404026
- [4] Turner, D., Lucieir, A., Wallace, L. 2014. Direct georeferencing of ultrahigh-resolution UAV imagery. *IEEE Transactions on Geoscience and Remote Sensing* 52(5), 2738-2745. DOI: 10.1109/TGRS.2013.2265295
- [5] Gupta, S.K., Shukla, D.P. 2018. Application of drone for landslide mapping, dimension estimation and its 3D reconstruction. *Journal of the Indian Society of Remote Sensing* 46(6), 903-914. DOI: 10.1007/s12524-017-0727-1
- [6] van der Sluijs, J., et al. 2018. Permafrost terrain dynamics and infrastructure impacts revealed by UAV photogrammetry and thermal imaging. *Remote Sensing* 10(11). DOI: 10.3390/rs10111734.
- [7] Niethammer, U., et al. 2011. Open source image-processing tools for low-cost UAV-based landslide investigations. in *International Archives of the Photogrammetry, Remote Sensing and Spatial Information Sciences - ISPRS Archives*.
- [8] Ham, Y., et al. 2016. Visual monitoring of civil infrastructure systems via camera-equipped Unmanned Aerial Vehicles (UAVs): a review of

- related works. *Visualization in Engineering* 4(1). DOI: 10.1186/s40327-015-0029-z
- [9] Siebert, S., Teizer, J. 2014. Mobile 3D mapping for surveying earthwork projects using an Unmanned Aerial Vehicle (UAV) system. *Automation in Construction* 41, 1-14. DOI: 10.1016/j.autcon.2014.01.004
- [10] Chen, J., et al. 2015. Open-pit mining geomorphic feature characterisation. *International Journal of Applied Earth Observation and Geoinformation* 42, 76-86. DOI: 10.1016/j.jag.2015.05.001
- [11] Suh, J., Choi, Y. 2017. Mapping hazardous mining-induced sinkhole subsidence using unmanned aerial vehicle (drone) photogrammetry. *Environmental Earth Sciences* 76(4). DOI: 10.1007/s12665-017-6458-3
- [12] Cara, S., Fiori, M., Matzuzzi, C. 2013. Assessment of landscape by photogrammetry proximity uav survey technique: A case study of an abandoned mine site in the Furtei area (Sardinia-Italy). in 23rd International Mining Congress and Exhibition of Turkey, IMCET 2013.
- [13] Kršák, B., et al. 2016. Use of low-cost UAV photogrammetry to analyze the accuracy of a digital elevation model in a case study. *Measurement: Journal of the International Measurement Confederation* 91, 276-287. DOI: 10.1016/j.measurement.2016.05.028
- [14] Shahbazi, M., et al. 2015. UAV-based point cloud generation for open-pit mine modelling. in *International Archives of the Photogrammetry, Remote Sensing and Spatial Information Sciences - ISPRS Archives*. DOI: 10.5194/isprsarchives-XL-1-W4-313-2015
- [15] Tong, X., et al. 2015. Integration of UAV-based photogrammetry and terrestrial laser scanning for the three-dimensional mapping and monitoring of open-pit mine areas. *Remote Sensing* 7(6), 6635-6662. DOI: 10.3390/rs70606635
- [16] Aicardi, I., et al. 2016. UAV photogrammetry with oblique images: First analysis on data acquisition and processing. in *International Archives of the Photogrammetry, Remote Sensing and Spatial Information Sciences - ISPRS Archives*. DOI: 10.5194/isprsarchives-XLI-B1-835-2016
- [17] Westoby, M.J., et al. 2012. 'Structure-from-Motion' photogrammetry: A low-cost, effective tool for geoscience applications. *Geomorphology* 179, 300-314. DOI: 10.1016/j.geomorph.2012.08.021
- [18] Sanz-Ablanedo, E., et al. 2018. Accuracy of Unmanned Aerial Vehicle (UAV) and SfM photogrammetry survey as a function of the number and location of ground control points used. *Remote Sensing* 10(10). DOI: 10.3390/rs10101606
- [19] Harwin, S., Lucieer, A. 2012. Assessing the accuracy of georeferenced point clouds produced via multi-view stereopsis from Unmanned Aerial Vehicle (UAV) imagery. *Remote Sensing* 4(6), 1573-1599. DOI: 10.3390/rs4061573.
- [20] Mancini, F., et al. 2013. Using unmanned aerial vehicles (UAV) for high-resolution reconstruction of topography: The structure from motion approach on coastal environments. *Remote Sensing* 5(12), 6880-6898. DOI: 10.3390/rs5126880
- [21] Trimble R10. Available online: <https://www.trimble.com/survey/trimble-r10.aspx> (accessed on 14/02/2020).
- [22] Gerke, M., Przybilla H.J. 2016. Accuracy analysis of photogrammetric UAV image blocks: Influence of onboard RTK-GNSS and cross flight patterns. *Photogrammetrie, Fernerkundung, Geoinformation* 2016(1), 17-30. DOI: 10.1127/pfg/2016/0284
- [23] Pix4D. Available online: <https://support.pix4d.com/hc/en-us/sections/360003718992-Manual> (accessed on 14/02/2020).
- [24] Agisoft. Available online: https://www.agisoft.com/pdf/photoscan-pro_1_4_en.pdf (accessed on 14/02/2020).
- [25] Zhou, Q. 2017. Digital Elevation Model and Digital Surface Model. *The International Encyclopedia of Geography*, John Wiley & Sons, Inc. 2017, pp 17. <https://doi.org/10.1002/9781118786352.wbieg0768>
- [26] Wilson, J.P., Gallant, J.C. 2000. *Terrain Analysis: Principles and Applications*. John Wiley & Sons, Inc. 2000.